sustainability

MDPI

Article

An Investigation of the Catalytic Activity of Inconel and Stainless Steel Powders in Reforming Primary Syngas

Claudia Bezerra Silva *, Michael Lugo-Pimentel, Carlos M. Ceballos and Jean-Michel Lavoie *

Laboratoire des Technologies de la Biomasse, Département de Génie Chimique et de Génie Biotechnologique, Faculté de Génie, Université de Sherbrooke, Sherbrooke, QC J1K 2R1, Canada; m.a.lugo00@gmail.com (M.L.-P.); carlos.mario.ceballos.marin@usherbrooke.ca (C.M.C.)

* Correspondence: claudia.bezerra.silva@usherbrooke.ca (C.B.S.); jean-michel.lavoie2@usherbrooke.ca (J.-M.L.)

Abstract: Biomass is perhaps the only renewable resource on the planet capable of delivering molecules similar to those derived from petroleum, and one of the most developed technologies to achieve this is gasification. When it comes to biomass conversion into fuels and commodities, supercritical water gasification (SCWG) could offer promising solution for producing hydrogen-rich syngas. However, the presence of methane (CH_4) and carbon dioxide (CO_2) in the syngas could negatively impact downstream processes, particularly when carbon monoxide is also required. Hence, improving the quality of the syngas produced from biomass gasification is essential for promoting the sustainability of several industrial processes. In this context, understanding the principles of the dry reforming of methane (DRM) becomes essential for upgrading syngas with high CH_4 and CO_2 content, especially when the carbon monoxide content is low. In addition to the experimental conditions used in such process, it has been reported that the material composition of the reactor can impact on reforming performance. Hence, this work aims at comparing the catalytic efficacy of Inconel and stainless steel for reforming syngas derived from SCWG under standard DRM conditions. In this specific work, the metals were directly used as catalyst and results showed that when using Inconel powder, CH_4 conversion increased from 3.03% to 37.67% while CO_2 conversion went from 23.16% to 51.48% when compared to stainless steel. Elemental and structural analyses revealed that the Inconel's superior performance might be due to its high nickel content and the formation of active oxide compounds, such as FeNiO, $FeCrO_3$, Fe_3O_4, Cr_2O_3, and Cr_2NiO_4, during the reaction. In contrast, Fe_3O_4 was the only oxide found in stainless steel post-reaction. Additionally, increasing the total gas feed flow rate was shown to reduce CH_4 and CO_2 conversions, supporting the known impact of residency time on catalytic efficiency.

Keywords: Inconel; stainless steel; catalytic activity; primary syngas reforming; sustainable energy

Academic Editor: Matthew Jones

Received: 2 November 2024
Revised: 27 December 2024
Accepted: 7 January 2025
Published: 25 January 2025

Citation: Bezerra Silva, C.; Lugo-Pimentel, M.; Ceballos, C.M.; Lavoie, J.-M. An Investigation of the Catalytic Activity of Inconel and Stainless Steel Powders in Reforming Primary Syngas. *Sustainability* **2025**, *17*, 980. https://doi.org/10.3390/su17030980

1. Introduction

Climate change is one of the most pressing global challenges, strongly influenced by our dependence on fossil fuels, which are a major source of greenhouse gas (GHG) emissions. Fossil fuel combustion alone contributes to approximately 24% of CO_2 emissions, causing extreme weather events, rising sea levels, and the degradation of ecosystems. Furthermore, increasing global energy demands are depleting oil, coal, and other non-renewable resources, making them increasingly difficult and costly to extract [1–3].

Syngas derived from renewable feedstock offers a promising building block for decarbonizing CO_2-intensive industries. Town gas is a versatile energy carrier and chemical

precursor that can be used for power generation in turbines or engines, for producing valuable chemical molecules, for hydrogen production, or as a building block for liquid fuels. These attributes make of syngas a critical actor in more sustainable industrial processes.

Amongst the different gasification processes, supercritical water gasification (SCWG) is particularly attractive for biomass conversion since it allows the production of hydrogen-rich syngas [4]. The latter could eventually represent an alternative approach to producing H_2 especially in the eventuality of putting forward a hydrogen-based economy. However, in addition to hydrogen, the syngas produced through SCWG contains other non-condensable gases such as methane (CH_4) and carbon dioxide CO_2 [5,6]. Such a situation could be of minimal impact if the gas is intended to be burnt or used for electricity production. However, having large amounts of CH_4 and CO_2 could be problematic for certain applications, such as the Fischer–Tropsch synthesis [7] and especially if these carbon compounds replace carbon monoxide in the mixture. To address this, syngas can go through upgrading steps to adjust the H_2/CO ratio. Hydrocarbon reforming technologies, such as dry reforming, are effective when residual alkanes (such as CH_4) and CO_2 are present in the raw syngas. The dry reforming is very endothermic hence it requires high energy in order to convert equimolar amounts of CH_4 and CO_2 to produce CO and H_2 at a 1:1 ratio (Equation (1)). However, depending on the operating conditions, several side reactions could occur, including (but not limited to) reverse water–gas shift (rWGS) (Equation (2)), CH_4 decomposition (Equation (3)), CO disproportionation (Equation (4)), and hydrogenation of CO_2 (Equation (5)) and/or CO (Equation (6)) [8,9].

$$CH_4 + CO_2 \leftrightarrow 2CO + 2H_2 \ (+247 \text{ kJ/mol}) \quad (1)$$

$$CO_2 + H_2 \leftrightarrow CO + H_2O \ (+41 \text{ kJ/mol}) \quad (2)$$

$$CH_4 \leftrightarrow C + 2H_2 \ (+75 \text{ kJ/mol}) \quad (3)$$

$$2CO \leftrightarrow C + CO_2 \ (-172 \text{ kJ/mol}) \quad (4)$$

$$CO_2 + 2H_2 \leftrightarrow C + 2H_2O \ (-90 \text{ kJ/mol}) \quad (5)$$

$$H_2 + CO \leftrightarrow H_2O + C \ (-131 \text{ kJ/mol}) \quad (6)$$

For applying DRM at an industrial scale, it is hence crucial to develop cost-efficient, highly active, and stable catalysts. These catalysts are key to improving the DRM efficiency by overcoming challenges such as the usually high-temperature requirements of the process [10,11]. As far as the catalyst is concerned the choice of its active metal(s) influences both the reaction performance as well as the catalyst activity. Distinct capacities to activate methane and carbon dioxide can be obtained depending on the metal, which directly affects the reaction rate. Noble metals have been reported for their high ability to break C–H bonds in methane while at the same time being up to a certain point refractory to coke formation, making them highly effective (and investigated) for DRM reactions. Metals such as iridium (Ir), ruthenium (Ru), rhodium (Rh), palladium (Pd), and platinum (Pt) are known for their excellent selectivity, stability, and catalytic activity. However, despite their catalytic properties, the high cost of these noble metals may become prohibitive for their industrial application, particularly for processes that require cost-effectiveness and catalyst regeneration [12,13]. Hence, nickel-based catalysts are very popular for dry reforming of methane due to their relatively low cost, extensive availability, and high catalytic activity. Their superior ability to break C-H bonds and their effectiveness in reforming reactions (they are commonly used for steam methane reforming processes) have made nickel-based catalysts sought after for commercial applications [14–16]. The metal, in addition to being a popular component of reforming catalyst, is also one of the main components of metal

alloys such as Inconel [17], which could make of such alloy a candidate as a catalyst as well. The catalytic effect of Inconel reactor walls was reported for different thermochemical processes where the higher catalytic effect was attributed to the material's high nickel content. Tuan Abdullah and Croiset [18] observed that Inconel-625 exhibits significant catalytic activity in ethanol reforming. Salierno et al. [19], when studying supercritical water gasification of glycerol, reported that the high nickel content in Inconel-625 reactors accelerates hydrogen consumption pathways, resulting in a 40% increase in methane production and a 50% reduction in hydrogen yield compared to stainless steel 316. Bustamante-Londono [20] reported that when using an Inconel reactor, much higher conversions for the water–gas shift reactions were achieved than in a quartz reactor, with up to 70 % conversions at higher temperatures. Finally, Zhu et al. found that nickel wire inside quartz reactors significantly improves gasification efficiency and the production of hydrogen during the supercritical water gasification of glycerol and glucose [21].

Building on prior work showcasing the impact of Inconel on DRM [22], this study aims to investigate the catalytic performance of this alloy as compared to stainless steel used as powders for the reforming of the raw syngas produced from supercritical water gasification (SCWG) of switchgrass (*Panicum virgatum*) which was originally composed of a majority of H_2, CO_2, and CH_4. Standard DRM conditions were applied to assess their impact on gas composition and conversion rates. Additionally, aims at investigating the changes in the elemental and crystalline structures of the catalysts post-reaction, providing insights into its stability and efficiency during high-temperature reforming processes.

2. Materials and Methods

The composition of the raw syngas used in this work replicates the output from the supercritical water gasification (SCWG) of Switch Grass (*Panicum virgatum*), that was performed at the Karlsruhe Institute of Technology (KIT) as part of the CERESiS project [23,24]. The gas mixture that was used in this research was directly inspired from the primary syngas produced for the SCWG of *Panicum virgatum* which involved 35 vol% H_2, 39 vol% CO_2, and 26 vol% CH_4. The conditions for dry reforming technology were applied to reform the gas. It was anticipated that the CH_4 and CO_2 in the gas were to react, yielding CO and additional H_2, as indicated by Equation (1). A simplified flow diagram of the reforming setup used in this work is depicted in Figure 1.

To have the desired composition of syngas at the inlet, a compressed gas cylinder was used for each component. Calibrated mass flow controllers allowed regulating the volumetric flow rate (mL/min) to achieve the desired composition in the feed, as shown in Figure 1. The gases used included hydrogen (H_2), methane (CH_4), and carbon dioxide (CO_2), as well as nitrogen (N_2) that was used as an internal standard since it should not be reacting under the reaction conditions and it does not participate in the DRM. This allows N_2 to be a reference point for accurately measuring the composition, variations in flow rates, and changes in the other gases during the reaction. All the gases (H_2, CO_2, CH_4, and N_2) were mixed and fed to the reactor at the top. The reactor was a clear fused quartz fixed-bed reactor, with 16 mm ID, 19 mm OD, and 304.8 mm length. It was heated by a vertical oven (260 mm tall, manufactured by Thermcraft, Winston-Salem, NC, USA) capable of reaching temperatures of up to 982 °C. Thermocouples were installed at different locations to monitor the oven and reactor temperatures.

The outlet gases produced during the reaction exited the reactor downstream. Due to the potential reverse water–gas shift reaction, a cold trap was installed immediately beneath the reactor outlet. This trap condensed and separated the water generated during the reaction, ensuring its removal from the gas phase for the accurate analysis of the remaining gaseous products. The trap consisted of an Erlenmeyer flask in an ice-filled container;

melted ice water was removed regularly and replaced to maintain a low temperature. Downstream of the cold trap, a metal flask filled with silica was used to retain condensable materials and prevent liquids from entering the gas samples.

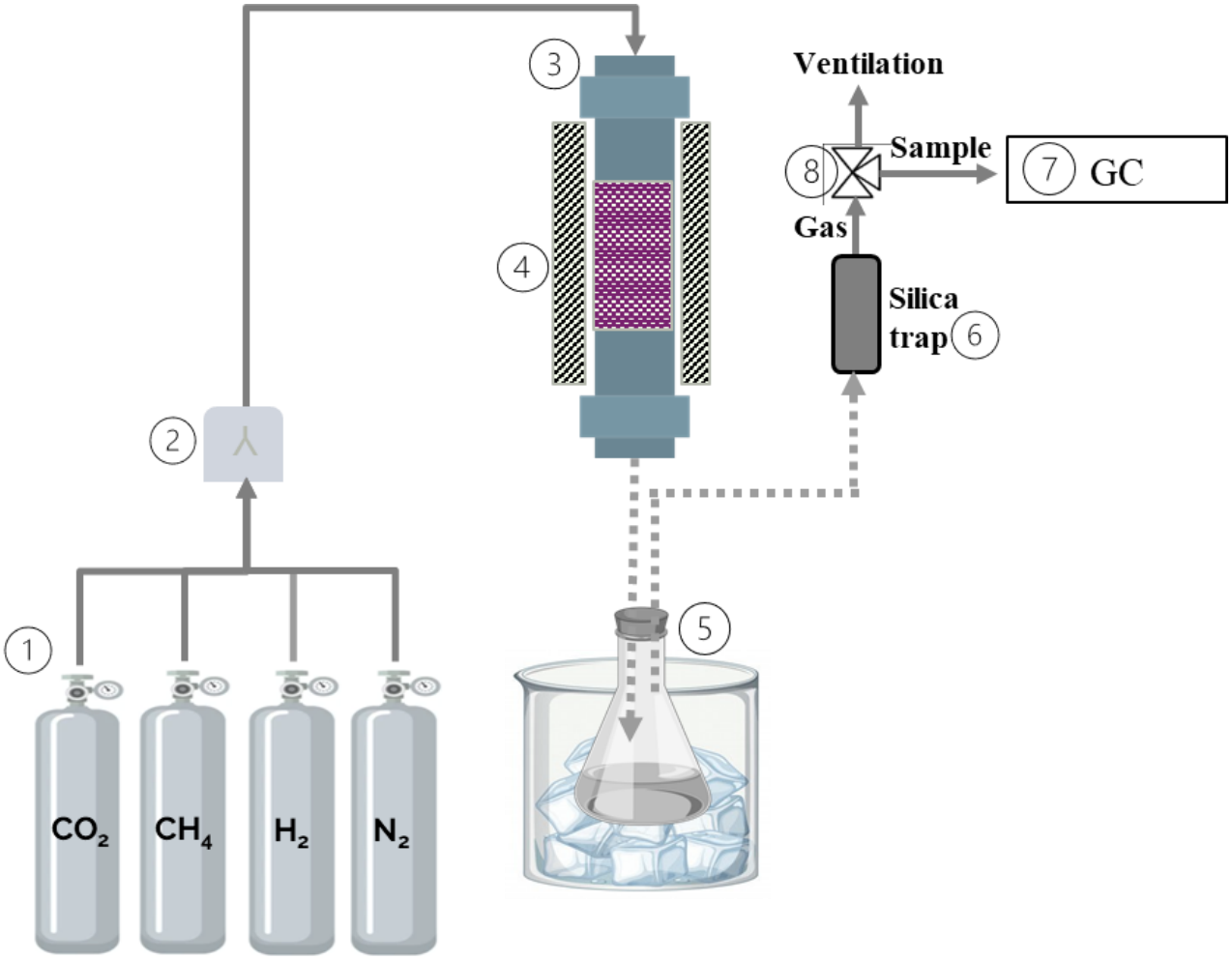

Figure 1. Simplified flow diagram of reforming setup (1: individual gas cylinders for CO_2, CH_4, H_2, and N_2; 2: static mixer; 3: glass reactor; 4: oven; 5: cold trap, consisting of an Erlenmeyer flask inside of a beaker filled with ice; 6: tube filled with silica; 7: gas chromatograph machine; 8: 3-way valve).

The reformed syngas was collected in appropriate sample bags (500 mL Tedlar bag with Polypropylene valve and septum fitting from Restek Corporation, Bellefonte, PA, USA) and analyzed using an Agilent 990 Micro Gas Chromatograph (GC), Santa Clara, CA, USA. This GC system featured two channels. Channel 1 used a 10 m Agilent J&W CP-Molesieve 5 Å column with backflush and RTS, designed to separate H_2, CO, CH_4, N_2, O_2, and some noble gases. Channel 2 employed a 10 m Agilent J&W CP-PoraPLOT U column with backflush, capable of detecting CO_2, ethane (C_2H_6), hydrogen sulfide (H_2S), and n-propene (C_3H_6).

Dry reforming typically occurs at elevated temperatures (generally 600 to 1000 °C) and atmospheric pressure [25,26]. Following this tendency, the reactions were conducted at 950 °C under atmospheric pressure and all tests conducted in this study had a duration of 5 h.

Two catalytic beds were tested for the process: one using Inconel 700 and the other on stainless steel 316 both in powder form. These powders were obtained by manually drilling tubes made of the respective materials using a diamond drill to obtain fine particles. Each catalyst consisted of 15 g of alloy (Inconel or stainless steel) powder combined with

21 g of alumina pellets. Alumina was used to increase the dispersion of the metal particles and extend the catalytic volume. Alumina also prevented sintering of the metal powders, which could otherwise agglomerate and reduce the effective catalytic surface area in the reactor. To assemble the reactor, a layer of quartz wool was placed at the bottom to hold the catalytic bed. The alumina pellets and metal powders were then alternately layered as uniformly as possible until the reactor was filled. Finally, a top layer of quartz wool was added to preserve the catalytic medium.

The catalyst beds were tested for their ability to reform the emulated raw syngas representing the one produced by SCWG. This study was divided into two parts: (I) comparing the catalytic activity of Inconel and stainless steel using a total raw syngas flow of 247 mL/min and (II) investigating the effect of increasing the total gas flow from 247 mL/min to 397 (as shown in Table 1), where the Inconel bed was employed for this part of the study.

Table 1. Total flow (mL/min) used in the second part of this work where Inconel powder was used as catalyst.

Condition	Total Flow (mL/min)
1	247
2	297
3	347
4	397

The performance of the catalysts was evaluated based on the conversions of CH_4 and CO_2, the percentage composition of the gas, and the H_2/CO ratio of the produced gas.

Equation (7) was used to calculate the percentage conversion of CH_4 and CO_2, where "i" represents either CH_4 or CO_2.

$$X_{(i)}(\%) = \frac{\text{Flow}_{\text{In}(i)} - \text{Flow}_{\text{Out}(i)}}{\text{Flow}_{\text{In}(i)}} \quad (7)$$

In this equation, $X_{(i)}(\%)$ corresponds to the percentage conversion of CH_4 or CO_2, calculated by comparing the difference between the molar flow rates of each one entering ($\text{Flow}_{\text{In}(i)}$) and exiting ($\text{Flow}_{\text{Out}(i)}$) the reactor to the initial flow rate ($\text{Flow}_{\text{In}(i)}$).

Analytical techniques such as Energy-Dispersive X-ray Spectroscopy (EDS) and X-ray Diffraction (XRD) were performed on the catalysts used in the reactions to gain a deeper understanding of their performance and the results observed.

EDS analyses were performed using a ThermoFisher Scientific Phenom XL G1 Desktop Scanning Electron Microscope (SEM) with Energy-Dispersive X-ray Spectroscopy (EDS) capabilities (Waltham, MA, USA). SEM was employed for high-resolution imaging and detailed morphological analysis. This technique facilitated a thorough examination of the elemental distribution on the sample's surface. Prior to analysis, the samples were embedded in epoxy resin, then cut and polished to achieve a low-roughness section. This preparation was crucial for precise mapping and quantitative analysis. Lastly, a thin gold coating was applied using sputter coating to prevent charging effects during the analysis.

To accurately identify crystalline phases, XRD analyses were performed on selected samples using the X'Pert Pro MPD diffractometer from Panalytical (Malver, UK). A copper (Cu) Kα radiation source with a wavelength of 1.54187 angstroms (Å) was used, and the 2θ measurement range extended from 15° to 80°. A step size of 0.04° was employed to capture finer details in the diffraction patterns, improving resolution. Each measurement lasted 260 s. The XRD analyses were conducted under stable conditions, with the instrument set to 40 kV and 50 mA. The diffraction data collected were processed and analyzed using the

JADE software (version 7.5.0, 2019) for the peak identification, phase quantification, and structural analysis of the crystalline phases in the samples.

3. Results

3.1. Part I: Inconel and Stainless Steel Activity

Figure 2 displays the gas composition at the inlet before and after the reforming experiments, using either stainless steel or Inconel powder as catalysts.

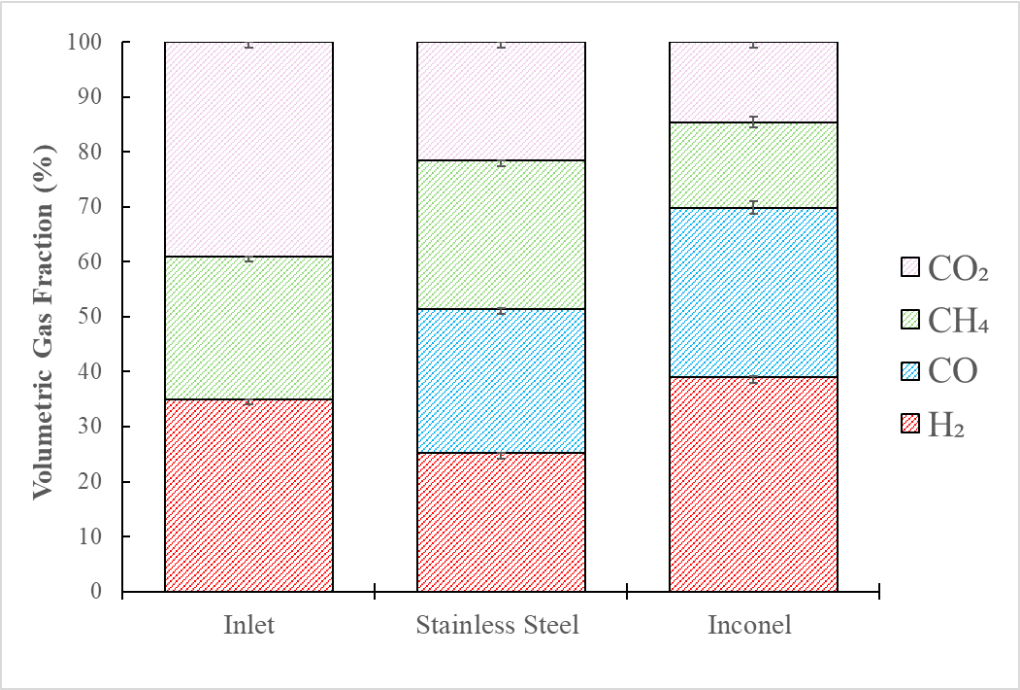

Figure 2. Gas composition (volumetric percentage) in the Inlet and reformed gas with stainless steel or Inconel powders (Reaction conditions: Inlet flow = 247 mL/min, 950 °C).

Figure 2 shows that when stainless steel powder was used as a catalyst, the gas produced consisted of less H_2 and CO but more CH_4 and CO_2 than Inconel. Further, Figure 2 shows that the quantity of H_2 increased with Inconel but decreased with stainless steel. This suggests that the stainless steel catalyst may have led to H_2 consumption due to the reverse water–gas shift reaction (Equation (3)). However, due to experimental limitations, it was not possible to measure the amount of water in the process, leaving the reverse water–gas shift reaction as a hypothesis. When using Inconel as catalyst results show that higher amounts of H_2 and CO were produced which could be an indication that the primary dry reforming reaction (Equation (3)) was facilitated by the Inconel reactor. The H_2/CO in the reformed gas for Inconel and stainless steel were 1.27 and 0.96, respectively. When a H_2/CO ratio of 1 is achieved in a dry reforming process, this could suggest that the reaction between CO_2 and CH_4 (dry reforming reaction) is the main one occurring, and although reactions that could favour H_2 and CO conversions are not impossible, they are likely less probable [27]. Considering that the feed of the process already had H_2, the H_2/CO of 0.96, along with the reduced amount of H_2 in the produced gas, shows that the dry reforming reaction was not the primary reaction happening in the presence of stainless steel. Figure 3 compares the CO_2 and CH_4 conversions after reforming when using stainless steel or Inconel as catalysts.

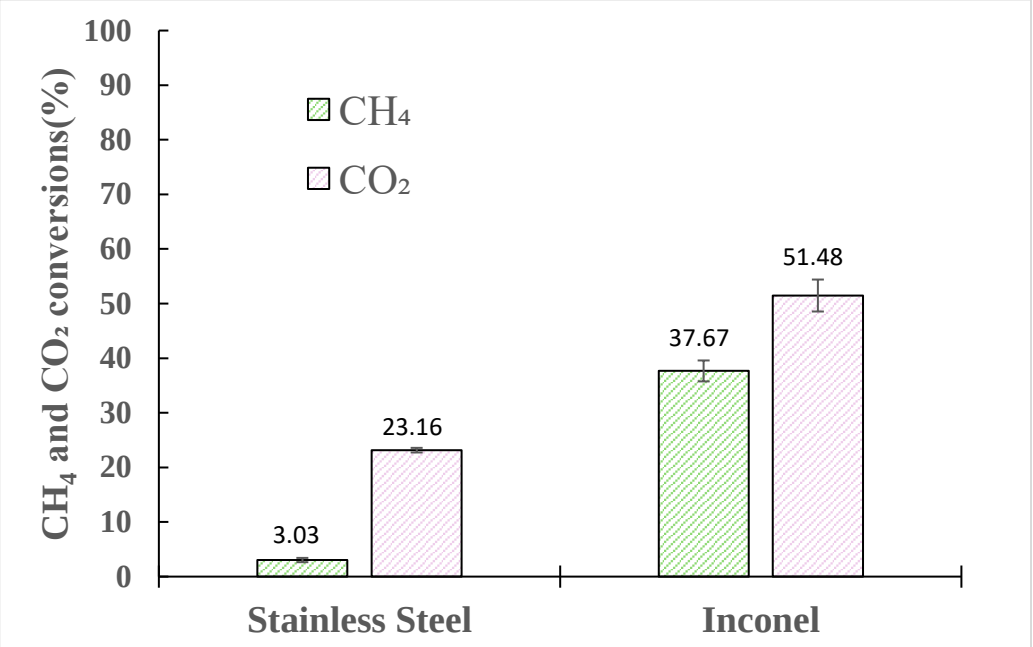

Figure 3. CO_2 and CH_4 conversions in the reformed gas using stainless steel or Inconel powder as catalyst (Reaction conditions: Inlet flow = 247 mL/min, 950 °C).

Figure 3 shows that CO_2 had a higher conversion rate for both catalysts than CH_4. The dissociation of CO_2 was better than CH_4, which might be related to the countless parallel reactions that may have facilitated the higher conversion of CO_2 [28]. Figure 3 also shows that using Inconel instead of stainless steel resulted in higher conversions of both CH_4 and CO_2. When switching from stainless steel to Inconel, CH_4 conversion increased approximately 12 times, whereas CO_2 conversion doubled. The Inconel alloys are mainly composed of nickel (in higher amounts), chromium, iron, as well as other minor amounts of other metals [29,30]. Nickel, for instance, has been well established as having promising activity for reactions such as for the dry reforming of methane (DRM) and has been known to facilitate cleavage of the C-H bond [31–33]. Moreover, some works have studied the influence of nickel alloy-based catalysts on this process. Several improvements have been observed when secondary or tertiary metals are alloyed with nickel catalysts, impacting on dispersion, reducibility, and leading to higher catalytic performance. Nickle alloys involving manganese, iron, cobalt, tin, copper, zinc, and indium are some examples that have already been studied and each had properties that could enhance the DRM process [34,35]. For example, the increase in reactivity observed by adding iron to nickel catalysts for the DRM process is believed to be due to the possible synergetic effect between the metals, the creation of more stable and active catalytic sites, and the creation of FeO oxides that could inhibit carbon deposition [36]. As an example, it has been reported that adding cobalt to nickel catalysts has enhanced carbon removal and the adsorption of surface oxygen [37]. It was also expected that combining several metals with nickel in the Inconel alloy could enhance its catalytic activity in reforming reactions. This enhanced activity would likely be higher than for the stainless-steel catalyst in the case of reforming reactions, since the latter is primarily composed of iron rather than nickel.

3.2. Analytical Analysis and Discussion

To gain further insights into the catalysts' activity and performance, analyses were conducted on the catalyst both before and after the reaction. However, although carbon deposition is a well-known issue that can significantly affect the performance of catalysts, its impact could not be directly assessed in this study since its quantification during the

experiments posed technical challenges, preventing accurate quantification. EDS and XRD analyses were performed and analyzed similarly to the approach reported by Bezerra Silva et al. [22]. Table 2 displays the EDS elemental analysis for a sample of the Inconel catalyst before and after the reaction.

Table 2. Elemental concentration generated by EDS analysis for the Inconel catalyst before and after the reaction (Reaction conditions: Inlet flow = 247 mL/min, 950 °C).

Element	Weight Concentration (%)	
	Before Reaction	After Reaction
Nickel	73.91	59.84
Chromium	16.55	13.40
Iron	8.68	7.10
Silicon	0.34	-
Oxygen	-	18.49
Manganese	0.27	0.53
Molybdenum	-	0.56
Titanium	0.25	0.08

As shown in Table 2, nickel is the primary element for both samples while the amount of iron and chromium was also as expected for a typical Inconel alloy. However, the big difference between both catalysts was the oxygen concentration, which increased significantly once the catalyst had been submitted to the reaction. The presence of oxygen after the reaction indicates that some of the metals found in the Inconel alloy might have been oxidized. In addition and as seen in Table 2, the concentration of some of the metals decreased after the reaction. This phenomenon occurs because the concentration values are shown in weight percentage, and logically, the oxygen incorporated (from oxidation) into the material after the reaction increased its total weight. Adding oxygen alters the composition, effectively reducing the relative weight percentages of metals such as nickel, chromium, and iron. As a result, while the absolute amounts of these metals may remain unchanged, their weight percentages decreased due to the increased total mass caused by the oxygen content. Figure 4 shows the Inconel sample after the reaction, emphasizing elemental analysis at four different zones.

The zones shown in Figure 4 were chosen due to the significant visual disparity observed among these four locations, which could indicate a different material composition in each zone. Thus, Table 3 shows the elemental analysis composition for these four zones.

Table 3. Elemental concentration generated by EDS analysis in four zones from Inconel catalyst after the reaction (Reaction conditions: Inlet flow = 247 mL/min, 950 °C).

Element	Weight Concentration (%)			
	Zone 1	Zone 2	Zone 3	Zone 4
Chromium	69.16	9.86	9.41	69.34
Oxygen	18.02	3.30	3.41	25.44
Manganese	9.48	0.08	0.07	2.20
Nickel	1.44	77.56	77.98	1.63
Titanium	0.89	0.05	0.03	0.75
Iron	0.57	8.32	8.49	0.22
Molybdenum	0.45	0.82	0.62	0.43

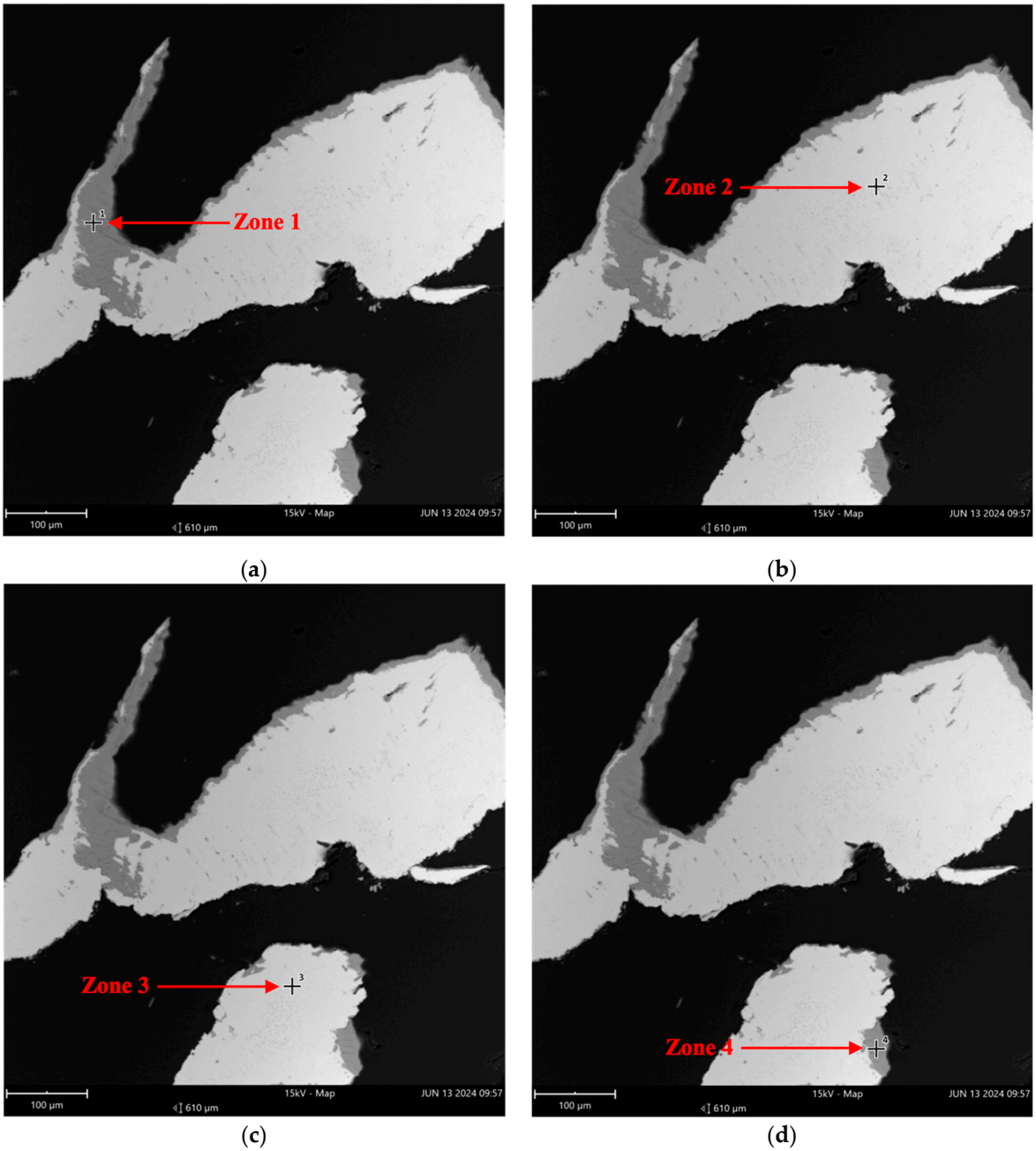

Figure 4. EDS analysis in four zones from a sample of the Inconel catalyst used in the reactions (**a**) zone 1, (**b**) zone 2, (**c**) zone 3, and (**d**) zone 4 (FOV: 963 µm, Mode: 15 kV—Point, Detector: BSD Full).

The elemental analysis for zones 1 and 4, presented in Table 3, shows that oxygen and chromium are the predominant elements, indicating the presence of chromium oxide, with almost no nickel observed. In contrast, zones 2 and 3 show high nickel content, followed by approximately 8% chromium and 8% oxygen, with significantly less oxygen than in zones 1 and 4. These results suggest the presence of pure nickel and chromium in zones 2 and 3. Despite the low oxygen concentration in these zones, different oxides are could also occur. To better understand the composition of the catalyst samples before and after the reaction, the same samples were analyzed by XRD, and the results are shown in Figure 5.

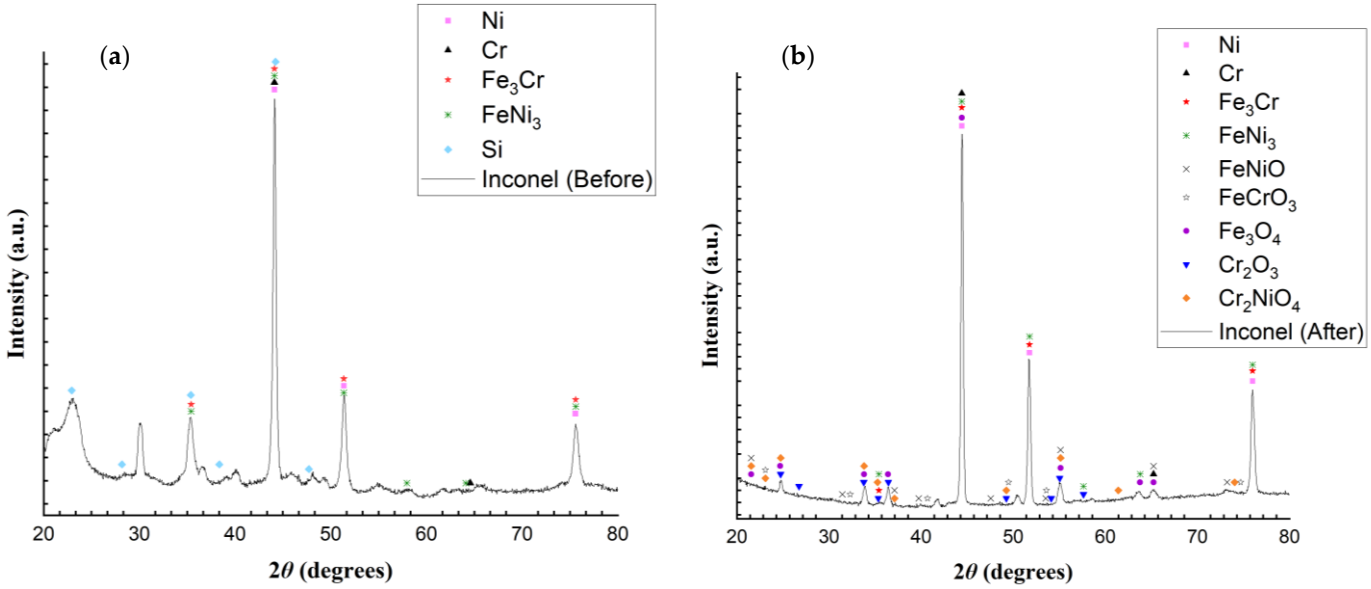

Figure 5. Diffractogram for Inconel catalyst (**a**) before and (**b**) after the reaction (Reaction conditions: Inlet flow = 247 mL/min, 950 °C).

The diffractograms of the fresh Inconel catalyst (Figure 5a) revealed peaks corresponding to pure nickel (2θ = 42.12, 51.37 and 75.57°), chromium (2θ = 42.12 and 64.57°), and silicon (2θ = 22.93, 28.17, 35.38, 38.36, 44.22 and 47.7187°), as well as compounds such as Fe_3Cr (2θ = 35.42, 44.12, 51.37 and 75.6°) and $FeNi_3$ (2θ = 35.42, 44.12, 51.36, 57.96, 64.12 and 75.6°). All diffraction peaks were identified using the internal database of the JADE software (version 7.5.0, 2019). These phases are consistent with the composition of Inconel, which primarily consists of Ni, Cr, and Fe. Fe_3Cr and $FeNi_3$ compounds suggest configurations of alloy that may arise during the manufacturing or the activation processes. Similar intermetallic phases have been reported in literature such as Jeyaprakash et al. [38] who identified $FeNi_3$, CoMn, and CoFe phases on Inconel-718, while Han et al. [39] reported a NiCr phase in Inconel 625. These studies highlighted the variability in phase formation depending on the specific alloy composition and thermal treatment. Noteworthy that the diffraction peaks will not perfectly match standard values since the Inconel alloy is complex. The latter contains different metals, which may result in several production phases with very similar or even the same peaks. This makes it difficult to understand the contribution that every single phase has in addition, intermetallic compound oxides add more complexity since they may diffract similarly. After the reaction (Figure 5b), the diffractogram revealed additional peaks corresponding to oxide compounds, including FeNiO (2θ = 21.54, 31.45, 37.11, 39.72, 47.55, 53.52, 55.15, 65.24, and 73.23°), $FeCrO_3$ (2θ = 23.09, 32.3, 40.70, 49.5, 53.6, and 74.69°), Fe_3O_4 (2θ = 21.541, 24.7, 33.8, 36.4, 44.42, 55.15, 63.77, and 65.24°), Cr_2O_3 (2θ = 24.75, 26.74, 33.78, 35.35, 36.44, 49.25, 54.13, 55.05, and 57.64°), and Cr_2NiO_4 (2θ = 21.54, 23.09, 24.75, 33.8, 35.26, 37.11, 49.25, 55.15, 61.41, and 74.03°). The formation of these oxides indicates significant oxidation during the reaction, which could alter the catalytic properties of the material. Oxidation likely occurred due to exposure to reactive gases at high temperatures, leading to the formation of an oxide layer on the surface. The coexistence of intermetallic and oxide phases underscores the dynamic nature of the catalyst under reaction conditions.

The reaction between pure Cr and CO_2 (Equation (8)) can produce Cr_2O_3, which, according to Contri et al. [40], could occur at approximately 750 °C.

$$2Cr + 3CO_2 \rightarrow Cr_2O_3 + 3CO \quad (8)$$

Equation (8) shows that the reaction between Cr and CO_2 also produces CO which could partly explain the increase of observed CO in the volumetric gas fraction when the Inconel catalyst was used instead of stainless steel, as shown in Figure 2. Cr_2O_3 formation can also occur by oxidizing pure chromium with O_2 and H_2O (Equations (9) and (10)) [41]. Both oxidizing agents are possibly present in the reaction medium, since O_2 could be produced as an intermediate of CO_2 dissociation, and H_2O could be produced by the reverse water–gas shift reaction (Equation (2)). For instance, Guo et al. demonstrated that the formation of Cr_2O_3 through chromium oxidation occurred in the presence of water, as described by Equation (10) [41].

$$2Cr + (3/2)O_2 \leftrightarrow Cr_2O_3 \quad (9)$$

$$2Cr + 3H_2O \rightarrow Cr_2O_3 + 3H_2 \quad (10)$$

Equation (10) also demonstrates the possibility of H_2 production, which could be one possible explanation for the H_2 increase when Inconel was used instead of stainless steel. Furthermore, studies on Ni-Cr-based catalysts used in dry reforming reactions have demonstrated that Cr_2O_3 can stabilize Ni active sites, thereby enhancing catalytic activity and increasing the conversion of CH_4 and CO_2 [42,43].

Although no Cr-Ni intermetallic bonds were identified before the reaction, the XRD in the catalyst post-reaction shows $CrNiO_4$, which could be produced by either reaction shown in Equations (11) and (12).

$$NiO + Cr_2O_3 \rightarrow Cr_2NiO_4 \quad (11)$$

$$Ni^{2+} + 2OH^- + Cr_2O_3 \rightarrow Cr_2NiO_4 + H_2O \quad (12)$$

FeNiO and $FeCrO_3$ oxides may either have resulted from the oxidation of intermetallic compounds present in the catalyst before the reaction or may also result from several other mechanisms involving iron, nickel, and chromium with an oxidizing agent.

Besides the significant nickel content in the Inconel catalyst, the oxides generated during the reaction likely contributed to higher CO_2 and CH_4 conversion rates as compared to the stainless-steel catalyst. The latter was also submitted to EDS elemental analysis at three different zones, and Table 4 shows the elemental analysis composition for these zones (see Figure 6).

Table 4. Elemental concentration generated by EDS analysis in tree zones from stainless steel catalyst after reaction (Reaction conditions: Inlet flow = 247 mL/min, 950 °C).

Element	Weight Concentration (%)		
	Zone 1	Zone 2	Zone 3
Iron	95.90	95.97	89.23
Oxygen	2.74	2.79	8.94
Manganese	0.74	0.71	0.99
Molybdenum	0.57	0.53	0.54
Chromium	0.03	-	-
Titanium	0.01	-	-

In Table 4, for all the zones, the elemental analysis shows that the post-reaction stainless steel catalyst is mostly composed of iron and oxygen, indicating the presence of iron oxide which was also confirmed by XRD as shown in Figure 7.

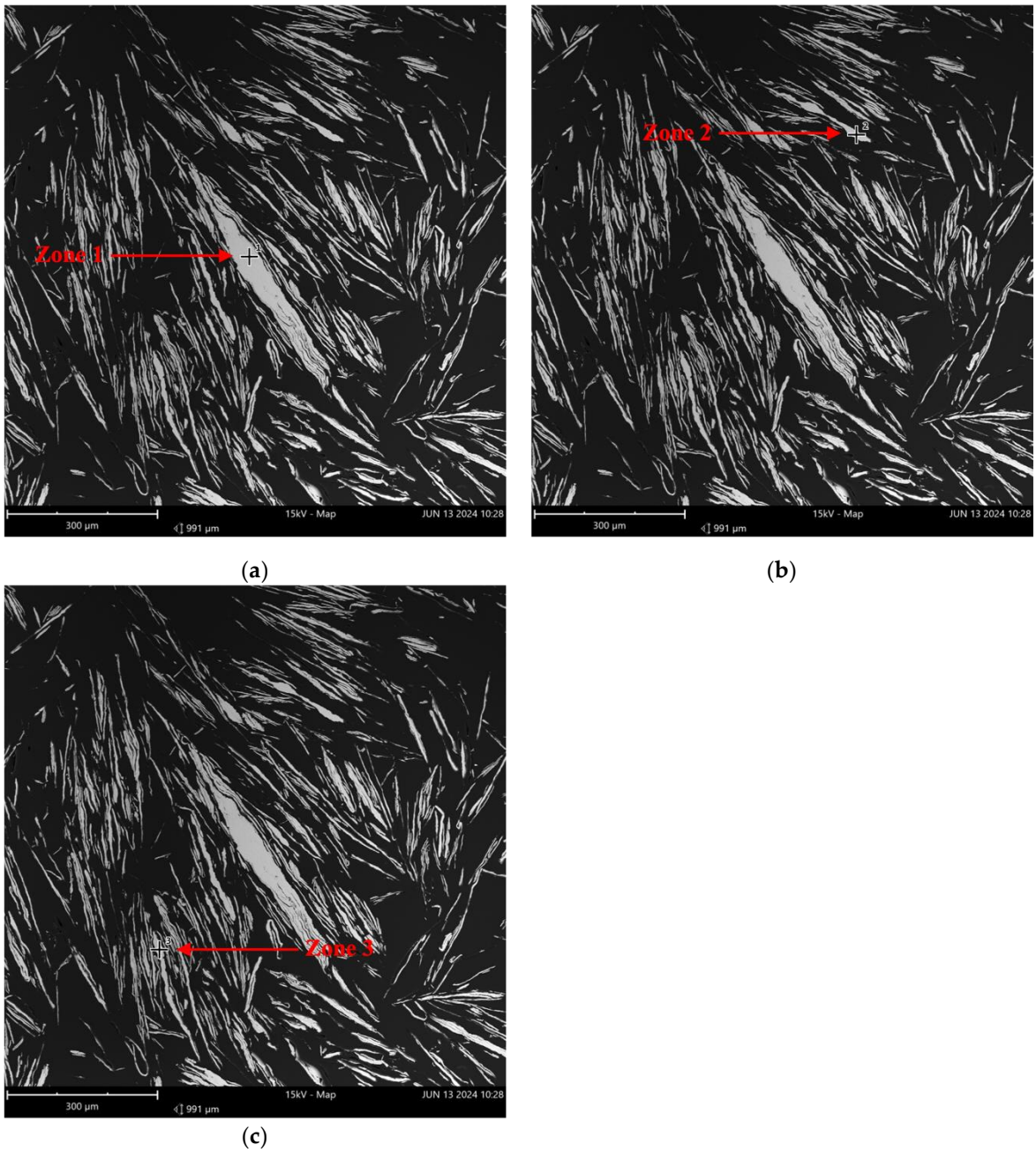

Figure 6. EDS analysis in 3 zones from stainless steel catalyst after reaction (**a**) zone 1, (**b**) zone 2, and (**c**) zone 3 (FOV: 991 µm, Mode: 15 kV—Map, Detector: BSD Full, Reaction conditions: Inlet flow = 247 mL/min, 950 °C).

The diffractogram in Figure 7 shows peaks corresponding to an iron–chromium compound (Fe_3Cr) as well as iron oxide Fe_3O_4. Although stainless steel is mainly composed of iron and chromium, iron–chromium can also be present in this material. The presence of Fe_3O_4 peaks indicates that the iron present in the catalyst was oxidized during the reaction.

Then, comparing both catalysts post-reaction, it is most likely that the higher activity of Inconel was due to its high nickel content and the oxides produced during the reaction, especially Cr_2O_3. In contrast, the stainless-steel analysis post-reaction included about 90% iron, followed by oxygen, and smaller amounts of manganese, molybdenum, chromium, and titanium. However, no nickel was found in this sample. Therefore, the lower stainless steel catalytic activity could be related to the absence of nickel or the combination of the other metals present in the alloy, which could be acting as a catalytic deactivator.

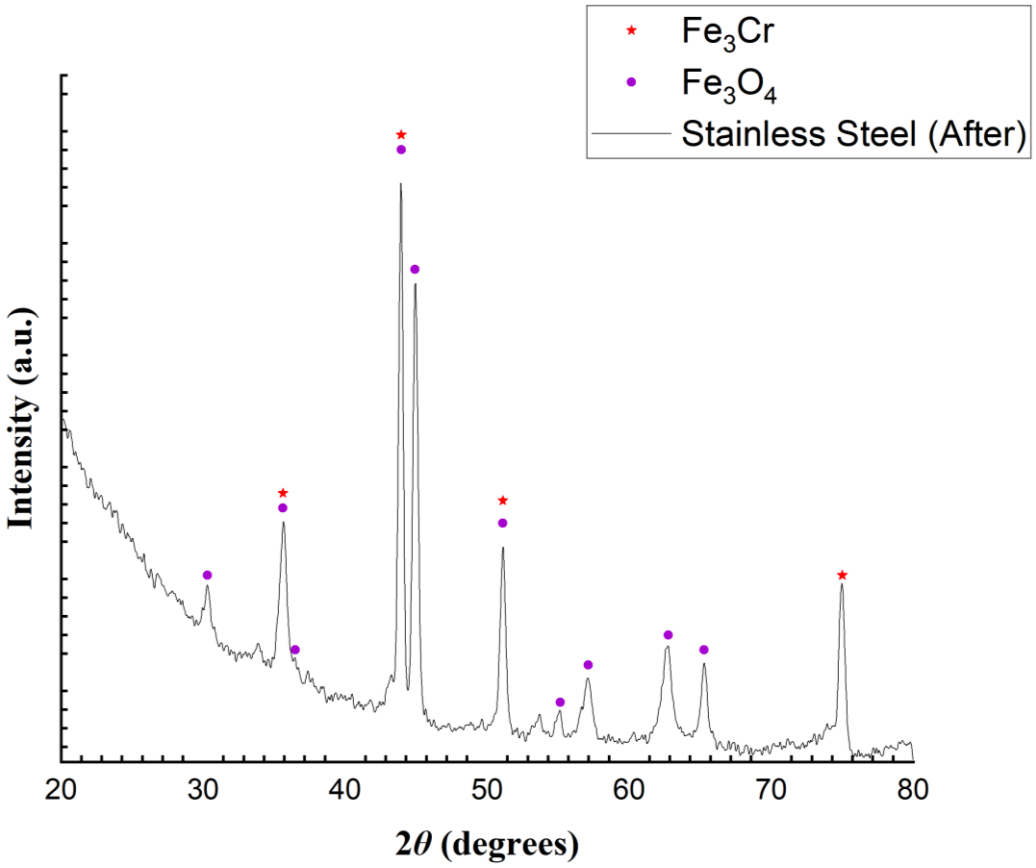

Figure 7. Diffractogram for stainless steel catalyst after the reaction (Reaction conditions: Inlet flow = 247 mL/min, 950 °C).

Inconel and stainless steel are common alloys, with their primary compositional difference being the high nickel (Ni) content in Inconel and the high iron (Fe) content in stainless steel, while both exhibit similar chromium (Cr) and molybdenum (Mo) levels. Nickel is well known for its catalytic properties in reforming primary syngas, however, it must remain in its metallic state to function effectively. Therefore, the other components of the alloy play a crucial role in ensuring this among which chromium and molybdenum are particularly recognized for their ability to significantly enhance metal oxidation and corrosion resistance under harsh conditions [44]. Chromium facilitates the formation of a stable passivation layer by promoting oxygen adsorption, as observed in ferritic stainless steel [45]. The addition of molybdenum to the alloys further improves corrosion resistance, particularly in acidic environments [46].

These findings align with the XRD results, which indicate that Cr is predominantly present as an oxide. This oxide layer protects Ni, ensuring it remains in its metallic state and continues to act as a catalyst. On the other hand, molybdenum was not identified in the XRD analysis. However, given its presence in the alloy, its behaviour as described in literature is consistent with the expected role of molybdenum in enhancing the alloy's performance under such conditions.

3.3. Part II: The Impact of Increasing the Total Gas Feed Flow (Inconel as Catalyst)

Figure 8 shows the gas composition at the inlet before and after the reforming experiments, using Inconel powder as a catalyst and using different flow feeds in the reactor.

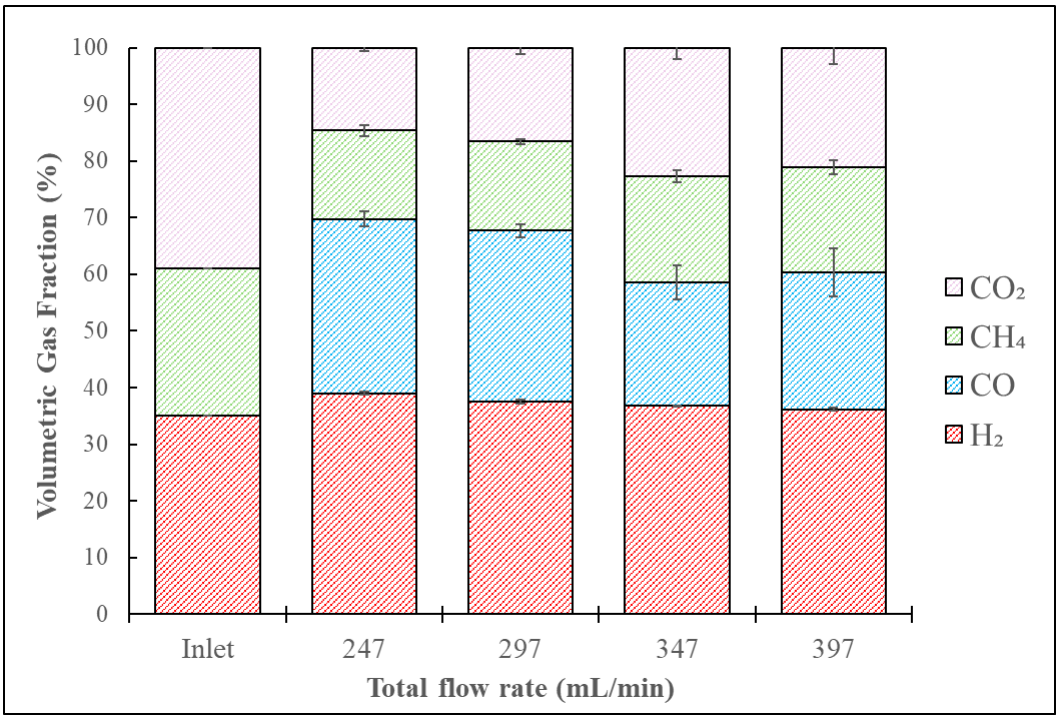

Figure 8. Gas composition (volumetric percentage) in the inlet and reformed gas with Inconel as catalyst at different total gas flow rates (Inlet flows tested: 247, 297, 347, and 397 mL/min, reaction temperature = 950 °C).

Figure 8 shows that H_2 increased while CH_4 and CO_2 concentrations decreased after reforming, compared to the inlet values for all tested total flow rates. When comparing the initial total flow rate of 247 mL/min with the higher flow rates tested, the increase slightly impacted the H_2 amounts, which showed a decreasing trend. CO_2 and CH_4 amounts, on the other hand, had more significant changes when the total flow was increased. The concentration of CO showed a decreasing trend up to the flow rate of 347 mL/min and slightly increased at 397 mL/min, though lower than at the 247 and 297 mL/min flows. Figure 9 compares the CO_2 and CH_4 conversions after reforming with Inconel at different total flow rates fed.

Figure 9 shows that the increase in the total flow rate decreased CH_4 and CO_2 conversions. This was expected since the catalytic bed volume remained constant, only the flow rate increased, and the Gas Hourly Space Velocity (GHSV) increased. When the GHSV increases, the gases flow faster inside the reactor, allowing the reacting molecules to spend less time interacting with the active sites on the catalyst while as well reducing adsorption and conversion [47]. Similar trend results in CH_4 and CO_2 conversions were found in the work of Jafarbegloo et al. [48], where both conversions decreased, along with the H_2/CO ratio, when the flow rate was increased. Table 5 shows the H_2/CO ratio results when changing the total flow rate from 247 to 367 mL/min.

Table 5. H_2/CO ratio for the reformed gas using Inconel as a catalyst, with the total flow rate varying from 247 to 397 mL/min (950 °C).

Total Flow (mL/min)	H_2/CO
247	1.27
297	1.25
347	1.68
397	1.50

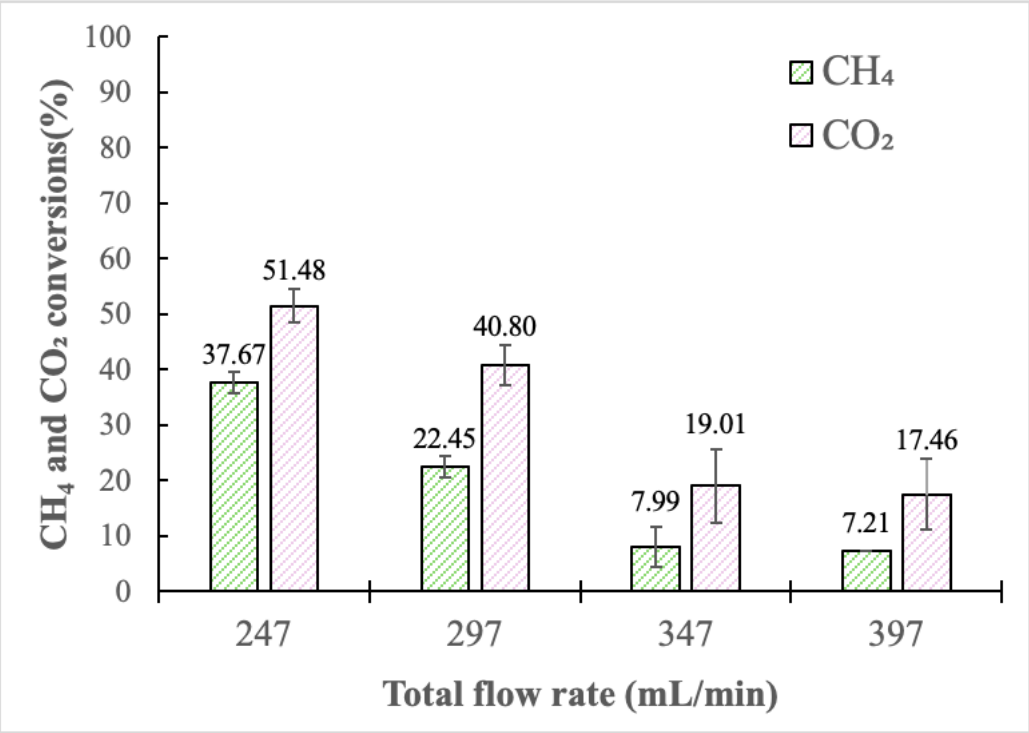

Figure 9. CO_2 and CH_4 conversions for the reformed gas with Inconel at different total flow rates (Inlet flows tested: 247, 297, 347, and 397 mL/min, reaction temperature = 950 °C).

As shown in Table 5, the increase in total flow did not significantly affect the H_2/CO ratio. Since the H_2 composition remained practically constant, variations in the H_2/CO ratio were primarily due to the changing amount of CO. This behaviour aligns with the findings of Choudhary et al. [49], who reported that changes in total flow had no substantial impact on the H_2/CO ratio.

Based on these results, it can be concluded that optimizing conversion efficiency is essential for any catalytic process. According to the analysis, optimizing gas flow rates is critical, as while the H_2/CO ratio remains unaffected, the conversions of CH_4 and CO_2 are significantly impacted. Longer contact times allow for better interaction between reactant gases and the active sites of the catalyst, maintaining overall process efficiency through higher conversion rates. Therefore, by controlling flow rates, optimal conditions for catalyst performance and longevity can be achieved, making catalytic processes both efficient and sustainable.

4. Conclusions

This work has demonstrated that the activity of Inconel when used as catalyst to reform raw SCWG syngas was higher than stainless-steel, which shows its potential for syngas upgrading. Results showed that the Inconel catalyst achieved higher conversion rates for both CO_2 and CH_4, which can be attributed to its high nickel content that can induce cleavage of C-H bonds. Moreover, the content of chromium itself and other metals present in Inconel contributed to the formation of active oxide compounds, such as Cr_2O_3, further enhancing catalytic activity. Another key finding of this work was the effect of the total gas feed flow rate on the performance of the Inconel catalyst. Higher flow rates led to reduced CH_4 and CO_2 conversions, likely due to shorter interaction times between gas molecules and the active sites of the catalyst. However, the H_2/CO ratio remained nearly constant despite changes in flow rate, with variation driven mainly by changes in CO production. The results of this study are relevant to the development of sustainable energy

systems since syngas, particularly when derived from biomass, could represent a critical building block for producing chemicals, energy, hydrogen, or liquid fuels. The catalysts evaluated in this work play a pivotal role in advancing these applications by potentially reducing dependence on fossil fuels while promoting the use of renewable feedstocks. Furthermore, the superior catalytic performance and durability of Inconel could lead to the creation of more efficient and robust systems, minimizing waste and operational costs. This contribution aligns with global efforts to develop energy-efficient processes and sustainable energy solutions.

Author Contributions: Conceptualization, C.B.S., M.L.-P. and J.-M.L.; methodology, C.B.S. and M.L.-P.; formal analysis, C.B.S., M.L.-P. and C.M.C.; investigation, C.B.S., M.L.-P. and C.M.C.; writing—original draft preparation, C.B.S. and M.L.-P.; writing—review and editing, C.M.C. and J.-M.L.; project administration, M.L.-P. and J.-M.L.; supervision, J.-M.L. All authors have read and agreed to the published version of the manuscript.

Funding: This research was funded by the Canadian New Frontiers in Research Fund under grant number NFRFG-2020-00148, the Canadian Fond de recherche Société et culture—Québec under grant number 308509, and the H2020 EU-Project CERESiS (Grant Agreement Nr.: 101006717).

Institutional Review Board Statement: Not applicable.

Informed Consent Statement: Not applicable.

Data Availability Statement: The raw data supporting the conclusions of this article will be made available by the authors upon request.

Acknowledgments: The authors would like to acknowledge the Université de Sherbrooke but more specifically the Biomass Technology Laboratory (BTL) for providing the infrastructure for this work as well as the Plateforme de recherche et d'analyse des matériaux (PRAM), for the analytical analyses. Additionally, the authors extend their gratitude to the EU H2020 project CERESiS for its support.

Conflicts of Interest: The authors declare no conflicts of interest.

References

1. Li, Y.; Guan, B.; Guo, J.; Chen, Y.; Ma, Z.; Zhuang, Z.; Zhu, C.; Dang, H.; Chen, L.; Shu, K.; et al. Renewable Synthetic Fuels: Research Progress and Development Trends. *J. Clean. Prod.* **2024**, *450*, 141849. [CrossRef]
2. Wojcieszyk, M.; Kroyan, Y.; Kaario, O.; Larmi, M. Prediction of Heavy-Duty Engine Performance for Renewable Fuels Based on Fuel Property Characteristics. *Energy* **2023**, *285*, 129494. [CrossRef]
3. Ebadi Torkayesh, A.; Hendiani, S.; Walther, G.; Venghaus, S. Fueling the Future: Overcoming the Barriers to Market Development of Renewable Fuels in Germany Using a Novel Analytical Approach. *Eur. J. Oper. Res.* **2024**, *316*, 1012–1033. [CrossRef]
4. Liu, S.; Yang, Y.; Yu, L.; Cao, Y.; Liu, X.; Yao, A.; Cao, Y. Self-Heating Optimization of Integrated System of Supercritical Water Gasification of Biomass for Power Generation Using Artificial Neural Network Combined with Process Simulation. *Energy* **2023**, *272*, 127134. [CrossRef]
5. Houcinat, I.; Outili, N.; García-Jarana, B.; Sánchez-Oneto, J.; Portela, J.R.; Meniai, A.H. Hydrogen Production by Supercritical Water Gasification: A Review. In *Renewable Energy Production and Distribution: Recent Developments*; Academic Press: Cambridge, MA, USA, 2022; pp. 189–225. [CrossRef]
6. Priya, A.; Naseem, S.; Pandey, D.; Bhowmick, A.; Attrah, M.; Dutta, K.; Rene, E.R.; Suman, S.K.; Daverey, A. Innovative Strategies in Algal Biomass Pretreatment for Biohydrogen Production. *Bioresour. Technol.* **2023**, *369*, 128446. [CrossRef] [PubMed]
7. Guilera, J.; Díaz-López, J.A.; Berenguer, A.; Biset-Peiró, M.; Andreu, T. Fischer-Tropsch Synthesis: Towards a Highly-Selective Catalyst by Lanthanide Promotion under Relevant CO_2 Syngas Mixtures. *Appl. Catal. A Gen.* **2022**, *629*, 118423. [CrossRef]
8. Huang, Y.; Li, X.; Zhang, Q.; Vinokurov, V.A.; Huang, W. Carbon Deposition Behaviors in Dry Reforming of CH4 at Elevated Pressures over Ni/MoCeZr/MgAl2O4-MgO Catalysts. *Fuel* **2022**, *310*, 122449. [CrossRef]
9. le Saché, E.; Reina, T.R. Analysis of Dry Reforming as Direct Route for Gas Phase CO_2 Conversion. The Past, the Present and Future of Catalytic DRM Technologies. *Prog. Energy Combust. Sci.* **2022**, *89*, 100970. [CrossRef]
10. Mosaad Awad, M.; Kotob, E.; Ahmed Taialla, O.; Hussain, I.; Ganiyu, S.A.; Alhooshani, K. Recent Developments and Current Trends on Catalytic Dry Reforming of Methane: Hydrogen Production, Thermodynamics Analysis, Techno Feasibility, and Machine Learning. *Energy Convers. Manag.* **2024**, *304*, 118252. [CrossRef]

11. Zhu, H.; Chen, H.; Zhang, M.; Liang, C.; Duan, L. Recent Advances in Promoting Dry Reforming of Methane Using Nickel-Based Catalysts. *Catal. Sci. Technol.* **2024**, *14*, 1712–1729. [CrossRef]
12. Tanimu, A.; Yusuf, B.O.; Lateef, S.; Tanimu, G.; Alhassan, A.M.; Azeez, M.O.; Alhooshani, K.; Ganiyu, S.A. Dry Reforming of Methane: Advances in Coke Mitigation Strategies via Siliceous Catalyst Formulations. *J. Environ. Chem. Eng.* **2024**, *12*, 113873. [CrossRef]
13. Nguyen, D.L.T.; Vy Tran, A.; Vo, D.V.N.; Tran Nguyen, H.; Rajamohan, N.; Trinh, T.H.; Nguyen, T.L.; Le, Q.V.; Nguyen, T.M. Methane Dry Reforming: A Catalyst Challenge Awaits. *J. Ind. Eng. Chem.* **2024**, *140*, 169–189. [CrossRef]
14. Guo, S.; Sun, Y.; Zhang, Y.; Zhang, C.; Li, Y.; Bai, J. Bimetallic Nickel-Cobalt Catalysts and Their Application in Dry Reforming Reaction of Methane. *Fuel* **2024**, *358*, 130290. [CrossRef]
15. Li, B.; Chen, H.; Yuan, X. Influence of Different La2O3 Loading on Hydroxyapatite Supported Nickel Catalysts in the Dry Reforming of Methane. *Fuel* **2024**, *369*, 131687. [CrossRef]
16. Zhang, L.; Wu, S.; Zhang, Y.; Ai, T.; Chen, D.; Luo, Y.; He, D. Constructing Thermally Stable Nickel Sub-Nanoparticles via in Situ Hydroxyl Trapping for Methane Dry Reforming. *Chem. Eng. J.* **2024**, *486*, 150337. [CrossRef]
17. Buddaraju, K.M.; Ravi Kiran Sastry, G.; Kosaraju, S. A Review on Turning of Inconel Alloys. *Mater. Today Proc.* **2021**, *44*, 2645–2652. [CrossRef]
18. Tuan Abdullah, T.A.; Croiset, E. Evaluation of an Inconel-625 Reactor and Its Wall Effects on Ethanol Reforming in Supercritical Water. *Ind. Eng. Chem. Res.* **2014**, *53*, 2121–2129. [CrossRef]
19. Salierno, G.; Marinelli, F.; Likozar, B.; Ghavami, N.; De Blasio, C. Supercritical Water Gasification of Glycerol: Continuous Reactor Kinetics and Transport Phenomena Modeling. *Int. J. Heat. Mass. Transf.* **2022**, *183*, 122200. [CrossRef]
20. Bustamante-Londono, F. *The High-Temperature, High-Pressure Homogeneous Water-Gas Shift Reaction in a Membrane Reactor*; University of Pittsburgh: Pittsburgh, PA, USA, 2004.
21. Zhu, C.; Wang, R.; Jin, H.; Lian, X.; Guo, L.; Huang, J. Supercritical Water Gasification of Glycerol and Glucose in Different Reactors: The Effect of Metal Wall. *Int. J. Hydrogen Energy* **2016**, *41*, 16002–16008. [CrossRef]
22. Bezerra Silva, C.; Lugo-Pimentel, M.; Ceballos, C.M.; Lavoie, J.M. Effect of the Reactor Material on the Reforming of Primary Syngas. *Molecules* **2024**, *29*, 5126. [CrossRef] [PubMed]
23. Dutzi, J.; Stoll, I.K.; Boukis, N.; Sauer, J. Screening of Ten Different Plants in the Process of Supercritical Water Gasification. *Sustain. Chem. Environ.* **2024**, *5*, 100062. [CrossRef]
24. CERESiS CERESiS: ContaminatEd Land Remediation through Energy Crops for Soil Improvement to Liquid Biofuel Strategies. Available online: https://ceresis.eu/ (accessed on 7 July 2024).
25. Leonzio, G.; Zondervan, E. Carbon Dioxide to Methanol: A Green Alternative to Fueling the Future. In *Reference Module in Chemistry, Molecular Sciences and Chemical Engineering*; Elsevier: Amsterdam, The Netherlands, 2024. [CrossRef]
26. Sedaghat, M.H.; Rahimpour, M.R. Computational Fluid Dynamics Simulation of Natural Gas Reformers. In *Advances in Synthesis Gas: Methods, Technologies and Applications: Volume 4: Syngas Process Modelling and Apparatus Simulation*; Elsevier: Amsterdam, The Netherlands, 2023; pp. 103–121. [CrossRef]
27. Lavoie, J.M. Review on Dry Reforming of Methane, a Potentially More Environmentally-Friendly Approach to the Increasing Natural Gas Exploitation. *Front. Chem.* **2014**, *2*, 81. [CrossRef] [PubMed]
28. Juan-Juan, J.; Román-Martínez, M.C.; Illán-Gómez, M.J. Effect of Potassium Content in the Activity of K-Promoted Ni/Al_2O_3 Catalysts for the Dry Reforming of Methane. *Appl Catal A Gen* **2006**, *301*, 9–15. [CrossRef]
29. Pavithran, N.R.; Harichandran, R.; Kumar, D.V. Effect of Yttria-Stabilized Zirconia Coating on the Corrosion and Thermal Behaviour of Additive Manufactured Inconel 718 Alloy. *J. Alloys Compd.* **2023**, *968*, 171877. [CrossRef]
30. Zhang, D.; Zhang, H.; Zhu, J.; Ding, M.; An, X.; Wu, D.; Hu, W.; Yang, T. High Strength-Ductility Synergy of Inconel 625 Alloy with a Layered Bimodal Grain-Structure. *Mater. Charact.* **2024**, *207*, 113510. [CrossRef]
31. Martín-Espejo, J.L.; Merkouri, L.P.; Gándara-Loe, J.; Odriozola, J.A.; Reina, T.R.; Pastor-Pérez, L. Nickel-Based Cerium Zirconate Inorganic Complex Structures for CO_2 Valorisation via Dry Reforming of Methane. *J. Environ. Sci.* **2024**, *140*, 12–23. [CrossRef]
32. Mosaad Awad, M.; Hussain, I.; Ahmed Taialla, O.; Ganiyu, S.A.; Alhooshani, K. Unveiling the Catalytic Performance of Unique Core-Fibrous Shell Silica-Lanthanum Oxide with Different Nickel Loadings for Dry Reforming of Methane. *Energy Convers. Manag.* **2024**, *311*, 118508. [CrossRef]
33. Miskan, S.N.; Abdulkadir, B.A.; Ainirazali, N.; Abd Jalil, A.; Lim, J.W.; Setiabudi, H.D. Unveiling the Effects of Nickel Loading on Methane Dry Reforming: Perspectives from Ni/Fibrous Zeolite-Y Catalysts. *Int. J. Hydrogen Energy*, 2024; *In press, Corrected Proof*. [CrossRef]
34. Torimoto, M.; Sekine, Y. Effects of Alloying for Steam or Dry Reforming of Methane: A Review of Recent Studies. *Catal. Sci. Technol.* **2022**, *12*, 3387–3411. [CrossRef]
35. Bian, Z.; Das, S.; Wai, M.H.; Hongmanorom, P.; Kawi, S. A Review on Bimetallic Nickel-Based Catalysts for CO_2 Reforming of Methane. *ChemPhysChem* **2017**, *18*, 3117–3134. [CrossRef]

36. Rao, Q.; Zhang, J.; Yang, T.; Li, Y.; Gai, Z.; Li, P.; Wang, X.; Pan, Y.; Jin, H. A Nickel-Modified Perovskite-Supported Iron Oxide Oxygen Carrier for Chemical Looping Dry Reforming of Methane for Syngas Production. *Chem. Eng. J.* **2024**, *485*, 150033. [CrossRef]
37. Sasson Bitters, J.; He, T.; Nestler, E.; Senanayake, S.D.; Chen, J.G.; Zhang, C. Utilizing Bimetallic Catalysts to Mitigate Coke Formation in Dry Reforming of Methane. *J. Energy Chem.* **2022**, *68*, 124–142. [CrossRef]
38. Jeyaprakash, N.; Yang, C.H.; Prabu, G.; Balamurugan, K.G. Surface Alloying of FeCoCrNiMn Particles on Inconel-718 Using Plasma-Transferred Arc Technique: Microstructure and Wear Characteristics. *RSC Adv.* **2021**, *11*, 28271–28285. [CrossRef] [PubMed]
39. Han, J.W.; Jung, S.H.; Cho, H.; Lee, H.W. Investigation of the Weld Properties of Inconel 625 Based on Nb Content. *Int. J. Electrochem. Sci.* **2018**, *13*, 2829–2841. [CrossRef] [PubMed]
40. Contri, B.; Valette, S.; Soustre, M.; Lefort, P. Inconel®625 Oxidation in CO_2: Kinetics and Reaction Mechanism. *Corros. Sci.* **2023**, *217*, 111101. [CrossRef]
41. Guo, S.; Xu, D.; Wei, N.; Wang, Y.; Chen, G.; Wang, S. Oxidation Processes and Involved Chemical Reactions of Corrosion-Resistant Alloys in Supercritical Water. *Ind. Eng. Chem. Res.* **2020**, *59*, 10278–10288. [CrossRef]
42. Bychkov, V.Y.; Korchak, V.N.; Krylov, O.V.; Morozova, O.S.; Khomenko, T.I. Formation of the Ni–CrOx/MgO and Ni/MgO Catalysts for Carbon Dioxide Reforming of Methane. *Kinet. Catal.* **2001**, *42*, 561–573. [CrossRef]
43. Rouibah, K.; Barama, A.; Benrabaa, R.; Guerrero-Caballero, J.; Kane, T.; Vannier, R.N.; Rubbens, A.; Löfberg, A. Dry Reforming of Methane on Nickel-Chrome, Nickel-Cobalt and Nickel-Manganese Catalysts. *Int. J. Hydrogen Energy* **2017**, *42*, 29725–29734. [CrossRef]
44. Hayes, J.R.; Gray, J.J.; Szmodis, A.W.; Orme, C.A. Influence of Chromium and Molybdenum on the Corrosion of Nickel-Based Alloys. *Corros. Sci.* **2006**, *62*, 491. [CrossRef]
45. Shen, Z. The Influence of Cr and Mo on the Formation of the Passivation Film on the Surface of Ferritic Stainless Steel. *Mater. Today Commun.* **2024**, *38*, 108221. [CrossRef]
46. Asami, K.; Naka, M.; Hashimoto, K.; Masumoto, T. Effect of Molybdenum on the Anodic Behavior of Amorphous Fe-Cr-Mo-B Alloys in Hydrochloric Acid. *Electrochem. Sci. Technol.* **1980**, *126*, 2130–2138. [CrossRef]
47. Abdullah, N.; Ainirazali, N.; Setiabudi, H.D.; Jalil, A.A.; Mohamed, A.R. Enhanced Glycerol Dry Reforming over Ni/SBA-15 Synthesized from Palm Oil Ash: Effect of GHSV. *Mater. Today Proc*, 2023; *In press, Corrected Proof*. [CrossRef]
48. Jafarbegloo, M.; Tarlani, A.; Mesbah, A.W.; Muzart, J.; Sahebdelfar, S. NiO-MgO Solid Solution Prepared by Sol-Gel Method as Precursor for Ni/MgO Methane Dry Reforming Catalyst: Effect of Calcination Temperature on Catalytic Performance. *Catal. Lett.* **2016**, *146*, 238–248. [CrossRef]
49. Choudhary, V.R.; Mondal, K.C.; Choudhary, T.V. Partial Oxidation of Methane to Syngas with or without Simultaneous Steam or CO_2 Reforming over a High-Temperature Stable-NiCoMgCeOx Supported on Zirconia–Hafnia Catalyst. *Appl. Catal. A Gen.* **2006**, *306*, 45–50. [CrossRef]